Phonon-Limited Valley Polarization in Transition-Metal Dichalcogenides

Zuzhang Lin,[1,2,3] Yizhou Liu,[4] Zun Wang,[2] Shengnan Xu,[2] Siyu Chen,[3] Wenhui Duan,[1,2,5,*] and Bartomeu Monserrat[3,6,†]

[1]*Institute for Advanced Study, Tsinghua University, Beijing 100084, China*
[2]*State Key Laboratory of Low Dimensional Quantum Physics and Department of Physics, Tsinghua University, Beijing 100084, China*
[3]*Cavendish Laboratory, University of Cambridge, JJ Thomson Avenue, Cambridge CB3 0HE, United Kingdom*
[4]*Department of Condensed Matter Physics, Weizmann Institute of Science, 7610001 Rehovot, Israel*
[5]*Frontier Science Center for Quantum Information, Beijing 100084, China*
[6]*Department of Materials Science and Metallurgy, University of Cambridge, 27 Charles Babbage Road, Cambridge CB3 0FS, United Kingdom*

(Received 1 February 2022; accepted 7 June 2022; published 5 July 2022)

The ability to selectively photoexcite at different Brillouin zone valleys forms the basis of valleytronics and other valley-related physics. Symmetry arguments combined with static lattice first-principles calculations suggest an ideal 100% valley polarization in transition-metal dichalcogenides under circularly polarized light. However, experimental reports of the valley polarization range from 32% to almost 100%. Possible explanations for this discrepancy include phonon-mediated transitions, which would place a fundamental limit to valley polarization, and defect-mediated transitions, which could, in principle, be reduced with cleaner samples. We explore the phonon-mediated fundamental limit by performing calculations of phonon-mediated optical absorption for circularly polarized light entirely from the first principles. We also use group theory to reveal the microscopic mechanisms behind the phonon-mediated excitations, discovering contributions from several individual phonon modes and from multiphonon processes. Overall, our calculations show that the phonon-limited valley polarization is around 70% at room temperature for state-of-the-art valleytronic materials including $MoSe_2$, MoS_2, WS_2, WSe_2, and $MoTe_2$. This fundamental limit implies that sufficiently pure transition-metal dichalcogenides are ideal candidates for valleytronics applications.

DOI: 10.1103/PhysRevLett.129.027401

Introduction.—Two-dimensional (2D) and few-layer transition-metal dichalcogenides (TMDs)—where spin, layer, and valley degrees of freedom can be exploited [1,2]—have brought revolutionary progress to fundamental physics and hold promise for technological advances. Of these, the manipulation of the valley degree of freedom to process and store information has given rise to the field of valleytronics [3–5], a promising approach to next-generation nanodevices. A circularly polarized optical field can drive an asymmetric distribution of carriers in the two valleys of TMDs [1], denoted as valley polarization. To make a valleytronics device, it is essential to generate a robust valley polarization [6–8].

Despite significant progress, the robustness of valley polarization in TMDs remains controversial. While *ab initio* simulations predict a valley polarization of almost 100% [9], consistent with selection rules, independent photoluminescence measurements have reported totally different values ranging from 32% to 100% [6,8–11], which are also temperature dependent. The inconsistency between experiment and theory and among different experiments can be ascribed to a combination of extrinsic effects, like a different concentration of defects in the samples [9,12] and intrinsic effects, in particular, phonon-assisted optical processes. While extrinsic effects could, in principle, be suppressed with purer samples, intrinsic phonon-assisted processes place a fundamental limit to valley polarization. Determining this fundamental limit is therefore critical for valleytronics applications.

In this Letter, we propose a new first-principles methodology to calculate phonon-assisted absorption for circularly polarized light and, with monolayer $MoSe_2$ as a representative TMD, use it to calculate the fundamental limit of valley polarization in TMDs. The transition matrix elements that are symmetry forbidden in the static crystal (i.e., without phonons) become symmetry allowed in the presence of phonons, thus suppressing valley polarization. We identify the dominant phonon modes suppressing valley polarization, and find that multiple phonon processes are important for these dynamically enabled transitions, resulting in an intrinsic valley polarization limit of 70% at room temperature in $MoSe_2$. More generally, the proposed first-principles methodology should be applicable to the study of finite-temperature optical absorption in other materials.

Phonon-limited valley polarization in TMDs.—Typical TMDs, such as $MoSe_2$, MoS_2, WS_2, WSe_2, and $MoTe_2$,

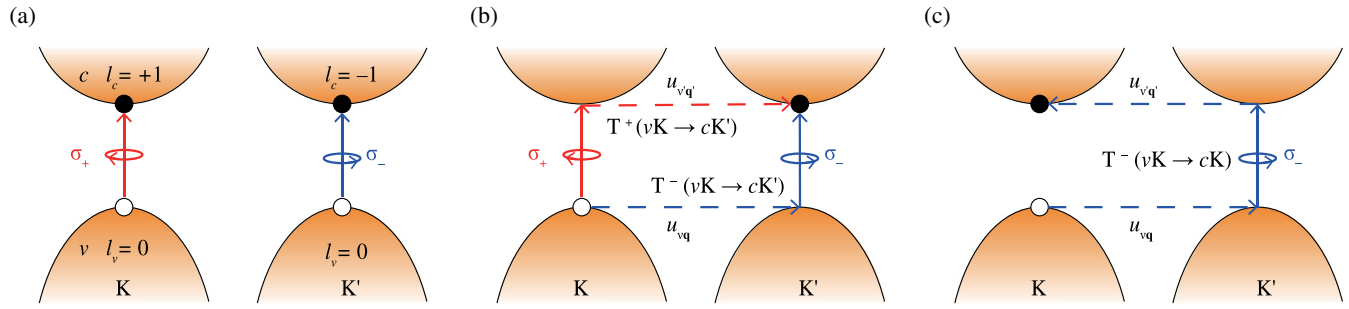

FIG. 1. (a) Valley contrasting circular optical transition rules with $\sigma_\pm$ referring to right(left)-handed polarized light. l_v (l_c) is the azimuthal quantum number of the conduction (valence) band. (b),(c) Valley contrasting rules are violated by phonon-assisted optical transitions. $T^\alpha(v\mathbf{k}_v \to c\mathbf{k}_c)$ represents a transition path from the valence band (v) with wave vector $\mathbf{k}_v$ to the conduction band (c) with wave vector $\mathbf{k}_c$ under light of helicity α ($\alpha = \pm$ refers to right- or left-handedness). The dashed lines refer to intervalley scatterings assisted by the phonon modes $u_{\nu\mathbf{q}}$ ($u_{\nu'\mathbf{q}'}$).

allow a valley contrasting circular dichroism between the $\mathbf{K}$ and $\mathbf{K}'$ valleys of the electronic structure [Fig. 1(a)] [13,14], which results in an ideal static valley polarization [9],

$$\eta_{\mathrm{sta}} = \frac{|\mathcal{P}^+_{cv}|^2 - |\mathcal{P}^-_{cv}|^2}{|\mathcal{P}^+_{cv}|^2 + |\mathcal{P}^-_{cv}|^2}. \tag{1}$$

Within the electric dipole approximation, the transition matrix elements $|\mathcal{P}^\pm_{cv}| = |\langle\psi_{c\mathbf{k}}|\hat{p}^\pm|\psi_{v\mathbf{k}}\rangle|$ describe the optical transition probability. Here, $\hat{p}^\pm = \hat{p}_x \pm i\hat{p}_y$ corresponds to right- (σ_+) or left-handed (σ_-) polarized light, and $|\psi_{v\mathbf{k}}\rangle$ and $|\psi_{c\mathbf{k}}\rangle$ represent the valence and conduction electronic states of crystal momentum $\mathbf{k}$, respectively. According to Eq. (1), incident light with fixed helicity will induce a 100% valley polarization with only states in one valley being excited. However, experimental measurements suggest values as low as 32% [6,8,9]. Such discrepancy may arise from two sources: (i) the imperfect crystal sample, e.g., defects which break crystal symmetry [9]; (ii) phonon scattering could enable otherwise forbidden transitions within and between valleys. While the former is extrinsic and could, in principle, be suppressed with purer samples, the latter is intrinsic and therefore impossible to remove.

To address this question, we study valley polarization including phonon-driven transitions, denoted as phonon-limited valley polarization. We use $T^\alpha(n\mathbf{k}_n \to m\mathbf{k}_m)$ to denote the possible transition of electrons from the state $n\mathbf{k}_n$ to $m\mathbf{k}_m$ under light with helicity α, where $n, m = v, c$ with v (c) representing valence (conduction) band state and $\mathbf{k}_n, \mathbf{k}_m = \mathbf{K}, \mathbf{K}'$ referring to the valley degrees of freedom. As an illustration, in Figs. 1(b) and 1(c) we show three transitions from the $\mathbf{K}$ valley, namely $T^+(v\mathbf{K} \to c\mathbf{K}')$, $T^-(v\mathbf{K} \to c\mathbf{K}')$, and $T^-(v\mathbf{K} \to c\mathbf{K})$, whose pathways will be carefully described later. Their conjugate transitions from the $\mathbf{K}'$ valley, namely $T^-(v\mathbf{K}' \to c\mathbf{K})$, $T^+(v\mathbf{K}' \to c\mathbf{K})$, and $T^+(v\mathbf{K}' \to c\mathbf{K}')$, are similar and not illustrated here. All six transitions are forbidden at the static lattice level (i.e., without phonons), which is the main reason behind the predicted perfect valley polarization. However, according to Fermi's golden rule in the framework of second-order perturbation theory [15,16], perfect valley polarization is lost, as these forbidden transitions can happen with the assistance of phonon-mediated processes via electron-phonon coupling (EPC) through intermediate states [17,18] [Figs. 1(b) and 1(c)]. Therefore, the expression in Eq. (1) no longer applies in the presence of phonons. To circumvent this, we define the phonon-limited valley polarization as

$$\begin{aligned}
\eta_\alpha(T) &= \frac{N_\alpha(\mathbf{K}) - N_\alpha(\mathbf{K}')}{N_\alpha(\mathbf{K}) + N_\alpha(\mathbf{K}')}, \\
N_\alpha(\mathbf{K}) &= |\mathcal{P}^\alpha(v\mathbf{K} \to c\mathbf{K})|^2 + |\mathcal{P}^\alpha(v\mathbf{K}' \to c\mathbf{K})|^2, \\
N_\alpha(\mathbf{K}') &= |\mathcal{P}^\alpha(v\mathbf{K} \to c\mathbf{K}')|^2 + |\mathcal{P}^\alpha(v\mathbf{K}' \to c\mathbf{K}')|^2,
\end{aligned} \tag{2}$$

where $\mathcal{P}^\alpha(v\mathbf{k}_v \to c\mathbf{k}_c)$ denotes the transition matrix element of the process $T^\alpha(v\mathbf{k}_v \to c\mathbf{k}_c)$ at finite temperature T ($\mathbf{k}_c, \mathbf{k}_v = \mathbf{K}, \mathbf{K}'$). Both intra- and intervalley processes are taken into account.

It should be noted that spin-flipping processes can also occur. The phonon-assisted paths (dashed lines) in Figs. 1(b) and 1(c) can be spin conserving or spin flipping. The EPC matrix element is given by [19]

$$\begin{aligned}
g^{\nu,\mathbf{q}}_{n,m,\mathbf{k}} &= \langle\psi_{m,\mathbf{k}+\mathbf{q}}|\frac{\partial V_{\mathrm{KS}}}{\partial u_{\nu\mathbf{q}}}|\psi_{n,\mathbf{k}}\rangle \\
&= \langle\psi_{m,\mathbf{k}+\mathbf{q}}|\frac{\partial V_{\mathrm{SC}}}{\partial u_{\nu\mathbf{q}}} + \frac{\partial V_{\mathrm{SF}}}{\partial u_{\nu\mathbf{q}}}|\psi_{n,\mathbf{k}}\rangle,
\end{aligned} \tag{3}$$

where V_{KS} is the Kohn-Sham potential, and V_{SC} and V_{SF} refer to its spin-conserving (SC) and spin-flipping (SF) parts, respectively. $u_{\nu\mathbf{q}}$ denotes the phonon mode of branch ν and wave vector $\mathbf{q}$. The spin-flipping potential V_{SF} contains spin-orbit coupling (SOC) terms, so that the spin-flipping processes arise as a result of the combined

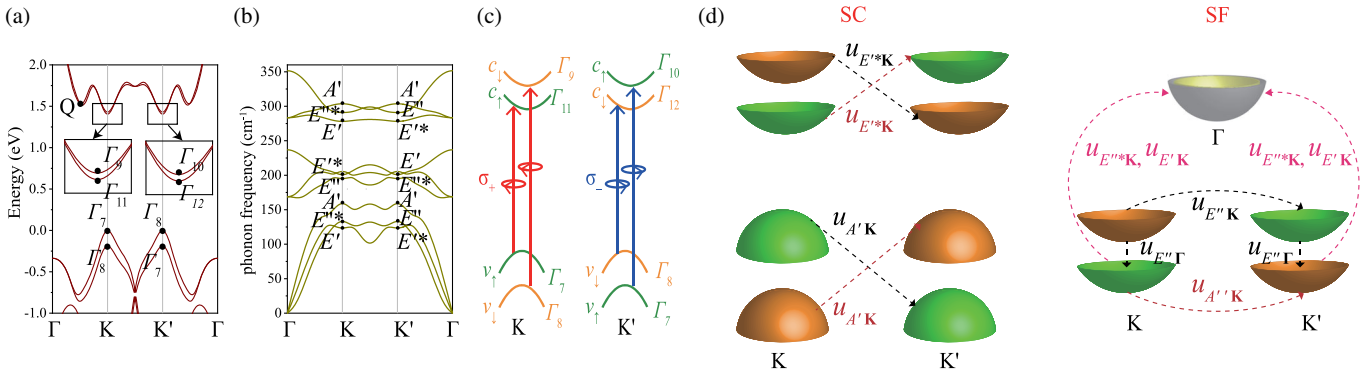

FIG. 2. (a) Electronic band structure and (b) phonon dispersion relation of monolayer $MoSe_2$ along high-symmetry lines with the corresponding IRs at high-symmetry points. The Γ_{7-12} refer to the double-valued representations of the little group C_{3h} at $\mathbf{K}$ and $\mathbf{K}'$ due to SOC, whereas the A', E', E'^*, E'', and E''^* refer to the single-valued representations of C_{3h}. $\mathbf{Q}$ is the midpoint between the $\mathbf{K}$ and $\mathbf{\Gamma}$ points. (c) Symmetry-allowed optical transition paths with the green (orange) curves representing spin-up (-down) electronic states at $\mathbf{K}$ ($\mathbf{K}'$) and the red (blue) lines representing a σ_+ (σ_-) photon. (d) Symmetry-allowed electron-phonon transition paths for SC (left) and SF (right) processes, respectively, with the dashed lines representing $u_{\mathbf{K}}$ (or $u_{\mathbf{K}'}$ whose IR is conjugate to $u_{\mathbf{K}}$) and $u_{\mathbf{\Gamma}}$ phonons.

effects of SOC and EPC. Hereafter, we will update the band indexes $n, m = v_\uparrow, v_\downarrow, c_\uparrow, c_\downarrow$ to include spin information.

Intra- and intervalley transitions in $MoSe_2$.—In the following, we investigate the phonon-limited valley polarization in monolayer $MoSe_2$. It has D_{3h} symmetry, whose single- and double-value representations are given in Ref. [20]. Figures 2(a) and 2(b) show the electronic band structure (including SOC) and phonon dispersion relation, respectively, along high-symmetry lines and including the irreducible representations (IRs) at high-symmetry points, which are consistent with earlier studies [1,21,22]. Monolayer $MoSe_2$ has a direct gap with conduction and valence band edges located at $\mathbf{K}$ and $\mathbf{K}'$. At the $\mathbf{K}$ point, the valence band with spin-up (-down) state has Γ_7 (Γ_8) symmetry; the conduction bands are nearly spin degenerate with the Γ_{11} (Γ_9) state having upward (downward) spin. The spin states at $\mathbf{K}'$ are opposite to those at $\mathbf{K}$ due to time-reversal symmetry.

For the valley-selective circular dichroism shown in Fig. 2(c), both SF and intervalley transitions are prohibited if only photons are included. However, the SF and intervalley transitions could be allowed by EPC and SOC processes with the symmetry-allowed intermediate phonons labeled in Fig. 2(d). The derivation details are given in Note S1 in the Supplemental Material [23]. The combination of photons and phonons gives rise to both intra- and intervalley excitations even with a fixed helicity of light.

Phonon-assisted transition amplitude from first principles.—To investigate the mechanism of phonon-limited valley polarization defined in Eq. (2), we first calculate

$$\Delta^{\alpha}_{cv}(\mathbf{q},\nu) = \frac{\hbar}{2\omega_{\nu\mathbf{q}}}\frac{\partial^2|\mathcal{P}^{\alpha}_{cv}|}{\partial u^2_{\nu\mathbf{q}}}, \tag{4}$$

which provides a quadratic approximation to the change $\Delta^{\alpha}_{cv}(\mathbf{q},\nu)$ in the transition matrix element induced by phonon mode $u_{\nu\mathbf{q}}$ [24]. This expression directly combines the contributions from photons and phonons in the transition. To evaluate Eq. (4), we generate atomic configurations in which phonon modes are excited individually [24] and use these to evaluate the second-order derivative of the transition matrix elements with a finite differences numerical scheme. At each atomic configuration, the transition matrix elements are directly calculated from response functions based on nonorthogonal localized orbitals (NOLOs) [25] as interfaced with OPENMX [26]. Additional details of the calculation method are described in Note S2 in the Supplemental Material [23].

We evaluate $\Delta^{\alpha}_{cv}(\mathbf{q},\nu)$ for $MoSe_2$, where depending on the initial state $|\psi_{v_\sigma\mathbf{k}_v}\rangle$ from the valence band and the final state $|\psi_{c_{\sigma'}\mathbf{k}_c}\rangle$ from the conduction band ($\sigma,\sigma' = \uparrow,\downarrow$), transitions can be divided into intra- and intervalley and into SC and SF, based on whether $\mathbf{k}_v = \mathbf{k}_c$ or $\sigma = \sigma'$. In the following, we focus on the intervalley SC transition $T^-(v_\uparrow\mathbf{K} \to c_\uparrow\mathbf{K}')$, the intervalley SF transition $T^+(v_\uparrow\mathbf{K} \to c_\downarrow\mathbf{K}')$, and the intravalley SC transition $T^-(v_\uparrow\mathbf{K} \to c_\uparrow\mathbf{K})$, all of which become possible with the mediation of phonons. We quantify the phonon correction to the transition matrix elements for the three transitions discussed above as a function of the phonon wave vector $\mathbf{q}$ throughout the Brillouin zone (BZ), i.e., $\Delta^{\alpha}_{cv}(\mathbf{q}) = \sum_\nu \Delta^{\alpha}_{cv}(\mathbf{q},\nu)$ [Figs. 3(a)–3(c)]. As expected, the $u_{\mathbf{K}}$ phonons drive large corrections since these phonons provide the required momentum (i.e., $\mathbf{K}$ or $-\mathbf{K}$) to connect the two valleys for the three transitions. In addition, we note that the $u_{\mathbf{\Gamma}}$ phonons dominate intravalley SF transition (Note S1 in the Supplemental Material [23]), which is also due to momentum conservation. Interestingly, we discover that the phonons near the $\mathbf{Q}$ point [the midpoint between the $\mathbf{K}$

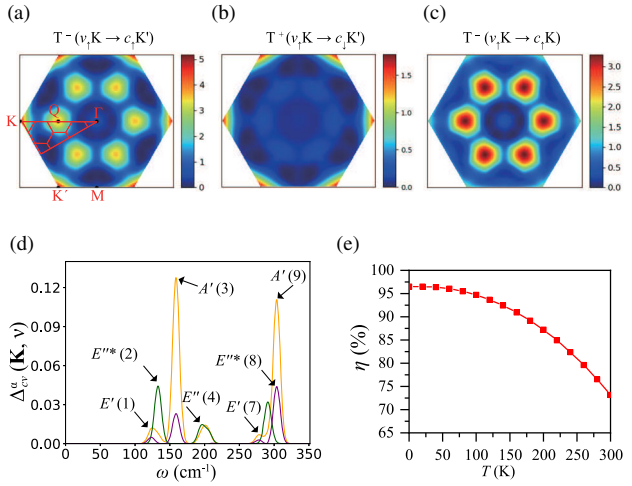

FIG. 3. (a)–(c) $\Delta^{\alpha}_{cv}(\mathbf{q})$ for (a) the intervalley-SC transition $T^{-}(v_{\uparrow}\mathbf{K} \to c_{\uparrow}\mathbf{K}')$, (b) the intervalley-SF transition $T^{+}(v_{\uparrow}\mathbf{K} \to c_{\downarrow}\mathbf{K}')$, and (c) the intravalley-SC transition $T^{-}(v_{\uparrow}\mathbf{K} \to c_{\uparrow}\mathbf{K})$. The red polygons in (a) represent the phonon sum weight in a 6×6 $\mathbf{q}$-point grid. (d) The $u_{\mathbf{K}}$ ($u_{\mathbf{K}'}$) phonon frequency resolved $\Delta^{\alpha}_{cv}(\mathbf{K},\nu)$ [$\Delta^{\alpha}_{cv}(\mathbf{K}',\nu)$] for the transitions $T^{-}(v_{\uparrow}\mathbf{K} \to c_{\uparrow}\mathbf{K}')$ (the orange curve), $T^{+}(v_{\uparrow}\mathbf{K} \to c_{\downarrow}\mathbf{K}')$ (the green curve) and $T^{-}(v_{\uparrow}\mathbf{K} \to c_{\uparrow}\mathbf{K})$ (the purple curve), which is given in arbitrary units. The corresponding IRs of the phonon peaks at the $\mathbf{K}$ point are labeled and the numbers in the brackets denote the number of phonon bands with increasing frequency. (e) The temperature dependent η calculated from the quadratic harmonic approximation, using a 6×6 $\mathbf{q}$-point grid.

and $\mathbf{\Gamma}$ points as shown in Fig. 2(a)] also make sizable contributions to the inter- and intravalley SC transitions $T^{-}(v_{\uparrow}\mathbf{K} \to c_{\uparrow}\mathbf{K}')$ and $T^{-}(v_{\uparrow}\mathbf{K} \to c_{\uparrow}\mathbf{K})$ [Figs. 3(a) and 3(c)]. According to momentum conservation, two $u_{\mathbf{Q}}$ phonons or one $u_{\mathbf{Q}}$ phonon plus one $u_{\mathbf{M}}$ phonon [Fig. 3(a)] are needed to make the intervalley transition possible. Our approach captures the two $u_{\mathbf{Q}}$ phonons transition, providing an example of a multiple phonon process that will be discussed in some detail later.

We show $\Delta^{\alpha}_{cv}(\mathbf{q},\nu)$ at $\mathbf{q} = \mathbf{K}$ as a function of the phonon frequency in Fig. 3(d). The numerically calculated $\Delta^{\alpha}_{cv}(\mathbf{q},\nu)$, together with the symmetry-derived selection rules in Fig. 2(d), help us determine the microscopic mechanism behind the phonon-limited valley polarization in TMDs. For example, as shown by the orange curve in Fig. 3(d), the two A' modes dominate in the SC intervalley transition $T^{-}(v_{\uparrow}\mathbf{K} \to c_{\uparrow}\mathbf{K}')$. Additionally, according to Fig. 2(d) the A' mode allows the intervalley transition from $v_{\uparrow}\mathbf{K}$ to $v_{\uparrow}\mathbf{K}'$, thus indicating the whole phonon-assisted transition path to be $v_{\uparrow}\mathbf{K} \to v_{\uparrow}\mathbf{K}' \to c_{\uparrow}\mathbf{K}'$. We also calculate the lowest-order electron-phonon matrix elements $|g^{\nu,\mathbf{q}}_{n,m,\mathbf{k}}|$ using the EPW code [27] to confirm that the $u_{A'\mathbf{K}}$ ($u_{A'\mathbf{K}'}$) phonons indeed contribute to the electron-phonon scattering path from $v_{\uparrow}\mathbf{K}$ to $v_{\uparrow}\mathbf{K}'$ (see Table S2 in the Supplemental Material [23]). The pathway for the SC transition $T^{-}(v_{\uparrow}\mathbf{K} \to c_{\uparrow}\mathbf{K})$ [Fig. 3(c)] can be determined in an analogous manner. For the SF transition [Fig. 3(b)], with a contribution smaller than that of the SC transitions, the pathway $c_{\uparrow}\mathbf{K} \to c_{\downarrow}\mathbf{K}'$ is not favorable because its symmetry-allowed phonon $u_{A''\mathbf{K}}$ does not have a significant contribution in Fig. 3(d), a result that is confirmed by the zero SF EPC matrix element [Eq. (3)] from the EPW calculations (Table S2 in the Supplemental Material [23]). We speculate that the dominant pathway for this SF transition may be $v_{\uparrow}\mathbf{K} \to c_{\uparrow}\mathbf{K} \to c\mathbf{\Gamma} \to c_{\downarrow}\mathbf{K}'$ because, for the path $c_{\uparrow}\mathbf{K} \to c\mathbf{\Gamma}$, a momentum $\mathbf{K}$ is needed and $u_{E''^{*}\mathbf{K}}$ [$u_{E''\mathbf{K}'}$] are symmetry-allowed phonon modes [Fig. 2(d)]. The SF intervalley scattering path via the Γ point was also reported before [28].

We now evaluate the phonon-limited valley polarization as a function of temperature by incorporating the thermal occupation of the phonon modes [23,24],

$$|\mathcal{P}^{\alpha}_{cv}| = |\mathcal{P}^{\alpha}_{cv}|_0 + |\Delta\mathcal{P}^{\alpha}_{cv}|,$$
$$|\Delta\mathcal{P}^{\alpha}_{cv}| = \sum_{\mathbf{q},\nu} \Delta^{\alpha}_{cv}(\mathbf{q},\nu)\left[\frac{1}{2} + n_B(\omega_{\nu\mathbf{q}},T)\right], \qquad (5)$$

where $|\mathcal{P}^{\alpha}_{cv}|_0$ is the transition matrix element in the absence of phonons, $\omega_{\nu\mathbf{q}}$ is the frequency of phonon mode $u_{\nu\mathbf{q}}$, and $n_B(\omega_{\nu\mathbf{q}},T)$ is the Bose-Einstein distribution function. The impact of temperature on the electron occupation is neglected, as the room temperature energy scale (~26 meV) is much smaller than the size of the electronic band gap (1.39 eV) in our simulations. Based on Eq. (5), we calculate the phonon-mediated transition matrix elements $|\mathcal{P}^{\alpha}_{cv}|$ in $MoSe_2$ by summing over the contribution from all phonons on a 6×6 $\mathbf{q}$ grid of the BZ. The sum can be limited to the irreducible BZ by assigning each phonon mode a weight that is proportional to the area of the polygon (see Note S3 in the Supplemental Material [23]) shown in Fig. 3(a) (that is the multiplicity of the $\mathbf{q}$ point).

The temperature-dependent phonon-limited valley polarization η is shown in Fig. 3(e). We find that η decreases with increasing temperature, driven by the increasing phonon occupation $n_B(\omega,T)$ and resulting in a reduced valley polarization of about 70% at 300 K—a lower bound in our estimation (see Notes S3 and S4 in the Supplemental Material [23]). We argue that the values of η in other TMDs should be similar to that of $MoSe_2$ because of the comparable band structure and EPC strength (Note S4 in the Supplemental Material [23]). Therefore, we can expect that TMDs exhibit high valley polarization even at room temperature, as long as the sample is pure enough, and thus are ideal candidates for valleytronics applications.

Discussion.—Beyond placing a fundamental limit to valley polarization, our analysis also allows us to rationalize some experimental reports of phonon-assisted processes in TMDs. Phonons that contribute to a virtual process

also dominate the corresponding real process because they follow the same symmetry constraints. The LA (**K**) phonon [the $A'(3)$ mode at the **K** point in Fig. 3(d)] was proposed to dominate the spin-conserved intervalley scattering in monolayer MoS_2 [40] (note MoS_2 has analogous properties to $MoSe_2$, so the results should be transferable). The ZA (**K**) phonon [the $E''^*(2)$ mode at the **K** point in Fig. 3(d)] which is clarified to effectively mediate the transition $T^+(v_\uparrow \mathbf{K} \to c_\downarrow \mathbf{K}')$ has been detected in spin-flip intervalley relaxations [41]. As for $u_\mathbf{Q}$ phonons, weak features around 380 [42] and 386 cm^{-1} [43] were observed in two previous low-temperature double-Raman experiments in bulk MoS_2, which might correspond to the contribution of acoustic phonons near the **Q** point [40].

Our results reveal the unexpectedly large contribution from $u_\mathbf{Q}$ phonons [Figs. 3(a) and 3(c)] in monolayer $MoSe_2$, which may be due to the special position of the **Q** point, which is a local (global) minimum of the conduction band of monolayer (bulk) $MoSe_2$. We discover that similar multiple phonon processes may also be considerable in other TMDs such as MoS_2, WS_2, WSe_2, and $MoTe_2$ (see Note S4 in the Supplemental Material [23]) and the important roles of $u_\mathbf{Q}$ phonons in bulk TMDs have been reported before [40,42,43]. We note that the $u_\mathbf{Q}$ phonons cause an increase of the transition matrix elements for the transition $T^-(v_\uparrow \mathbf{K} \to c_\uparrow \mathbf{K})$ [Fig. 3(c)], which suggests that terms beyond lowest-order perturbation theory are important, an observation that has also been reported in other materials [44].

The first-principles study of phonon-assisted optical processes has only recently become possible. While previous studies have reported phonon-assisted absorption across indirect band gaps using linear response methods [15] and finite difference methods [45], and across dipole-forbidden transitions using finite difference methods [18], our Letter provides the first calculation of phonon-assisted transitions with a circularly polarized optical field. It should be noted that our NOLO-based approach, which does not use Wannier interpolation [46,47], enables high throughput calculations for many atomic configurations. Moreover, our approach could be extended with a stochastic Monte Carlo scheme [23,24] to incorporate arbitrary orders of EPC strength and could also be extended to include a higher-level description of electrons (beyond the independent-particle approximation) or phonons (including anharmonic effects).

In conclusion, we calculate the phonon-induced fundamental limit of valley polarization in TMDs, which is larger than 70% at room temperature. This may set a standard for valleytronics applications. The electron-phonon scattering pathway traced out for several transitions could be used to design optical processes in which specific phonons are targeted, thus providing a road map for optical control of phonons. For example, it may guide the design of optical processes to excite specific anharmonic phonons beyond infrared-active phonons to achieve ultrafast lattice control [48–53]. We emphasize that the combination of the NOLO scheme for calculating electronic transitions with the finite difference approach for evaluating phonons and electron-phonon interactions provides a general approach to study phonon-assisted processes in various linear and nonlinear responses in condensed matter physics, including shift current conductivity, orbital magnetization, and the nonlinear Hall effect. Future works on these areas are highly anticipated.

This work was supported by the Basic Science Center Project of NSFC (Grant No. 51788104) and the Beijing Advanced Innovation Center for Future Chip. S. C. acknowledges financial support from the Cambridge Trust and from the Winton Programme for the Physics of Sustainability. B. M. acknowledges support from a UKRI Future Leaders Fellowship (Grant No. MR/V023926/1), from the Gianna Angelopoulos Programme for Science, Technology, and Innovation, and from the Winton Programme for the Physics of Sustainability.

*duanw@mail.tsinghua.edu.cn
†bm418@cam.ac.uk

[1] D. Xiao, G.-B. Liu, W. Feng, X. Xu, and W. Yao, Coupled Spin and Valley Physics in Monolayers of MoS_2 and Other Group-VI Dichalcogenides, Phys. Rev. Lett. **108**, 196802 (2012).
[2] Z. Gong, G.-B. Liu, H. Yu, D. Xiao, X. Cui, X. Xu, and W. Yao, Magnetoelectric effects and valley-controlled spin quantum gates in transition metal dichalcogenide bilayers, Nat. Commun. **4**, 2053 (2013).
[3] Z. Zhu, A. Collaudin, B. Fauqué, W. Kang, and K. Behnia, Field-induced polarization of Dirac valleys in bismuth, Nat. Phys. **8**, 89 (2012).
[4] T. Cai, S. A. Yang, X. Li, F. Zhang, J. Shi, W. Yao, and Q. Niu, Magnetic control of the valley degree of freedom of massive Dirac fermions with application to transition metal dichalcogenides, Phys. Rev. B **88**, 115140 (2013).
[5] Z.-M. Yu, S. Guan, X.-L. Sheng, W. Gao, and S. A. Yang, Valley-Layer Coupling: A New Design Principle for Valleytronics, Phys. Rev. Lett. **124**, 037701 (2020).
[6] H. Zeng, J. Dai, W. Yao, D. Xiao, and X. Cui, Valley polarization in MoS_2 monolayers by optical pumping, Nat. Nanotechnol. **7**, 490 (2012).
[7] O. Gunawan, Y. P. Shkolnikov, K. Vakili, T. Gokmen, E. P. De Poortere, and M. Shayegan, Valley Susceptibility of an Interacting Two-Dimensional Electron System, Phys. Rev. Lett. **97**, 186404 (2006).
[8] K. F. Mak, K. He, J. Shan, and T. F. Heinz, Control of valley polarization in monolayer MoS_2 by optical helicity, Nat. Nanotechnol. **7**, 494 (2012).
[9] T. Cao, G. Wang, W. Han, H. Ye, C. Zhu, J. Shi, Q. Niu, P. Tan, E. Wang, B. Liu *et al.*, Valley-selective circular dichroism of monolayer molybdenum disulphide, Nat. Commun. **3**, 1 (2012).

[10] G. Sallen, L. Bouet, X. Marie, G. Wang, C. Zhu, W. Han, Y. Lu, P. Tan, T. Amand, B. Liu, and B. Urbaszek, Robust optical emission polarization in MoS_2 monolayers through selective valley excitation, Phys. Rev. B **86**, 081301(R) (2012).

[11] S. Liu, A. Granados del Águila, X. Liu, Y. Zhu, Y. Han, A. Chaturvedi, P. Gong, H. Yu, H. Zhang, W. Yao, and Q. Xiong, Room-temperature valley polarization in atomically thin semiconductors via chalcogenide alloying, ACS Nano **14**, 9873 (2020).

[12] G. Kioseoglou, A. Hanbicki, M. Currie, A. Friedman, D. Gunlycke, and B. Jonker, Valley polarization and intervalley scattering in monolayer MoS_2, Appl. Phys. Lett. **101**, 221907 (2012).

[13] D. Xiao, W. Yao, and Q. Niu, Valley-Contrasting Physics in Graphene: Magnetic Moment and Topological Transport, Phys. Rev. Lett. **99**, 236809 (2007).

[14] W. Yao, D. Xiao, and Q. Niu, Valley-dependent optoelectronics from inversion symmetry breaking, Phys. Rev. B **77**, 235406 (2008).

[15] J. Noffsinger, E. Kioupakis, C. G. Van de Walle, S. G. Louie, and M. L. Cohen, Phonon-Assisted Optical Absorption in Silicon from First Principles, Phys. Rev. Lett. **108**, 167402 (2012).

[16] M. Cardona and Y. Y. Peter, *Fundamentals of Semiconductors* (Springer, New York, 2005).

[17] G. F. Bassani and G. P. Parravicini, *Electronic States and Optical Transitions in Solids* (Pergamon, New York, 1975), Vol. 8.

[18] A. J. Morris and B. Monserrat, Optical absorption driven by dynamical symmetry breaking in indium oxide, Phys. Rev. B **98**, 161203(R) (2018).

[19] F. Giustino, Electron-phonon interactions from first principles, Rev. Mod. Phys. **89**, 015003 (2017).

[20] C. Bradley and A. Cracknell, *The Mathematical Theory of Symmetry in Solids: Representation Theory for Point Groups and Space Groups* (Oxford University Press, Oxford, 2009).

[21] Y. Song and H. Dery, Transport Theory of Monolayer Transition-Metal Dichalcogenides through Symmetry, Phys. Rev. Lett. **111**, 026601 (2013).

[22] S. Horzum, H. Sahin, S. Cahangirov, P. Cudazzo, A. Rubio, T. Serin, and F. M. Peeters, Phonon softening and direct to indirect band gap crossover in strained single-layer $MoSe_2$, Phys. Rev. B **87**, 125415 (2013).

[23] See Supplemental Material at http://link.aps.org/supplemental/10.1103/PhysRevLett.129.027401 for selection rules of optical absorption, methodology, the estimate of the lower bound of valley polarization, discussion for other transition-metal dichalcogenides, and tests for other exchange-correlation functionals, which includes Refs. [19,24–39].

[24] B. Monserrat, Electron–phonon coupling from finite differences, J. Phys. Condens. Matter **30**, 083001 (2018).

[25] C. Wang, S. Zhao, X. Guo, X. Ren, B.-L. Gu, Y. Xu, and W. Duan, First-principles calculation of optical responses based on nonorthogonal localized orbitals, New J. Phys. **21**, 093001 (2019).

[26] T. Ozaki, K. Nishio, and H. Kino, Efficient implementation of the nonequilibrium green function method for electronic transport calculations, Phys. Rev. B **81**, 035116 (2010).

[27] J. Noffsinger, F. Giustino, B. D. Malone, C.-H. Park, S. G. Louie, and M. L. Cohen, EPW: A program for calculating the electron–phonon coupling using maximally localized Wannier functions, Comput. Phys. Commun. **181**, 2140 (2010).

[28] S. Xu, C. Si, Y. Li, B.-L. Gu, and W. Duan, Valley depolarization dynamics in monolayer transition-metal dichalcogenides: Role of the satellite valley, Nano Lett. **21**, 1785 (2021).

[29] K. Kunc and R. M. Martin, Ab Initio Force Constants of GaAs: A New Approach to Calculation of Phonons and Dielectric Properties, Phys. Rev. Lett. **48**, 406 (1982).

[30] J. H. Lloyd-Williams and B. Monserrat, Lattice dynamics and electron-phonon coupling calculations using nondiagonal supercells, Phys. Rev. B **92**, 184301 (2015).

[31] T. Ozaki, Variationally optimized atomic orbitals for large-scale electronic structures, Phys. Rev. B **67**, 155108 (2003).

[32] G. Theurich and N. A. Hill, Self-consistent treatment of spin-orbit coupling in solids using relativistic fully separable ab initio pseudopotentials, Phys. Rev. B **64**, 073106 (2001).

[33] J. P. Perdew, K. Burke, and M. Ernzerhof, Generalized Gradient Approximation Made Simple, Phys. Rev. Lett. **77**, 3865 (1996).

[34] S. Baroni, S. De Gironcoli, A. Dal Corso, and P. Giannozzi, Phonons and related crystal properties from density-functional perturbation theory, Rev. Mod. Phys. **73**, 515 (2001).

[35] P. Giannozzi, S. Baroni, N. Bonini, M. Calandra, R. Car, C. Cavazzoni, D. Ceresoli, G. L. Chiarotti, M. Cococcioni, I. Dabo *et al.*, QUANTUM ESPRESSO: A modular and open-source software project for quantum simulations of materials, J. Phys. Condens. Matter **21**, 395502 (2009).

[36] D. R. Hamann, Optimized norm-conserving Vanderbilt pseudopotentials, Phys. Rev. B **88**, 085117 (2013).

[37] F. Bassani, G. P. Parravicini, R. A. Ballinger, and J. L. Birman, *Electronic States and Optical Transitions in Solids* (Pergamon Press, New York, 1975), pp. 149–176.

[38] J. P. Perdew and Y. Wang, Accurate and simple analytic representation of the electron-gas correlation energy, Phys. Rev. B **45**, 13244 (1992).

[39] D. M. Ceperley and B. J. Alder, Ground State of the Electron Gas by a Stochastic Method, Phys. Rev. Lett. **45**, 566 (1980).

[40] B. R. Carvalho, Y. Wang, S. Mignuzzi, D. Roy, M. Terrones, C. Fantini, V. H. Crespi, L. M. Malard, and M. A. Pimenta, Intervalley scattering by acoustic phonons in two-dimensional MoS_2 revealed by double-resonance Raman spectroscopy, Nat. Commun. **8**, 14670 (2017).

[41] T.-Y. Jeong, S. Bae, S.-Y. Lee, S. Jung, Y.-H. Kim, and K.-J. Yee, Valley depolarization in monolayer transition-metal dichalcogenides with zone-corner acoustic phonons, Nanoscale **12**, 22487 (2020).

[42] T. Sekine, K. Uchinokura, T. Nakashizu, E. Matsuura, and R. Yoshizaki, Dispersive Raman mode of layered compound 2H-MoS_2 under the resonant condition, J. Phys. Soc. Jpn. **53**, 811 (1984).

[43] T. Livneh and J. E. Spanier, A comprehensive multiphonon spectral analysis in MoS_2, 2D Mater. **2**, 035003 (2015).

[44] N.-E. Lee, J.-J. Zhou, H.-Y. Chen, and M. Bernardi, Ab initio electron-two-phonon scattering in GaAs from next-to-leading order perturbation theory, Nat. Commun. **11**, 1 (2020).

[45] C. E. Patrick and F. Giustino, Unified theory of electron-phonon renormalization and phonon-assisted optical absorption, J. Phys. Condens. Matter **26**, 365503 (2014).

[46] I. Souza, N. Marzari, and D. Vanderbilt, Maximally localized Wannier functions for entangled energy bands, Phys. Rev. B **65**, 035109 (2001).

[47] N. Marzari and D. Vanderbilt, Maximally localized generalized Wannier functions for composite energy bands, Phys. Rev. B **56**, 12847 (1997).

[48] D. Afanasiev, J. Hortensius, B. Ivanov, A. Sasani, E. Bousquet, Y. Blanter, R. Mikhaylovskiy, A. Kimel, and A. Caviglia, Ultrafast control of magnetic interactions via light-driven phonons, Nat. Mater. **20**, 607 (2021).

[49] R. Mankowsky, A. von Hoegen, M. Först, and A. Cavalleri, Ultrafast Reversal of the Ferroelectric Polarization, Phys. Rev. Lett. **118**, 197601 (2017).

[50] T. Nova, A. Disa, M. Fechner, and A. Cavalleri, Metastable ferroelectricity in optically strained $SrTiO_3$, Science **364**, 1075 (2019).

[51] D. Fausti, R. Tobey, N. Dean, S. Kaiser, A. Dienst, M. C. Hoffmann, S. Pyon, T. Takayama, H. Takagi, and A. Cavalleri, Light-induced superconductivity in a stripe-ordered cuprate, Science **331**, 189 (2011).

[52] R. Mankowsky, A. Subedi, M. Först, S. O. Mariager, M. Chollet, H. Lemke, J. S. Robinson, J. M. Glownia, M. P. Minitti, A. Frano *et al.*, Nonlinear lattice dynamics as a basis for enhanced superconductivity in $YBa_2Cu_3O_{6.5}$, Nature (London) **516**, 71 (2014).

[53] M. Rini, R. Tobey, N. Dean, J. Itatani, Y. Tomioka, Y. Tokura, R. W. Schoenlein, A. Cavalleri, Control of the electronic phase of a manganite by mode-selective vibrational excitation, Nature (London) **449**, 72 (2007).